Nuclear Physics A471 (1987) 131c-148c
North-Holland, Amsterdam

THE ANGULAR MOMENTUM DEPENDENCE OF COMPLEX FRAGMENT EMISSION

L.G. SOBOTKA, D.G. SARANTITES, ZE LI and E.L. DINES

Department of Chemistry, Washington University, St. Louis, MO 63130

M.L. HALBERT and D.C. HENSLEY

Oak Ridge National Laboratory, Oak Ridge, TN 37830

R.P. SCHMITT, Z. MAJKA and G. NEBBIA

Texas A and M University, College Station, TX 77843

H.C. GRIFFIN

University of Michigan, Ann Arbor, MI 48109

A.J. SIERK

Los Alamos National Laboratory, Los Alamos, NM 87545

Large fragment (A>4) production at high angular momentum is studied via the reaction, 200 MeV ^{45}Sc + ^{65}Cu. Comparisons of the fragment yields from this reaction (high angular momentum) to those from ^{93}Nb + Be (low angular momentum) are used to verify the strong angular momentum dependence of large fragment production predicted by equilibrium models. Details of the coincident γ-ray distributions not only confirm a rigidly rotating intermediate but also indicate that the widths of the primary L-wave distributions decrease with increasing symmetry in the decay channel. These data are used to test the asymmetry and L-wave dependence of emission barriers calculated from a rotating, finite range corrected, liquid drop model.

I. INTRODUCTION

The object of studying heavy ion induced fission is to determine the magnitude and L-wave dependence of the fission barrier. For any value of the angular momentum the symmetric fission barrier can be considered as the central point in an ion-ion potential energy surface which extends into the mass asymmetry degree of freedom. It is this potential energy surface which determines the fate of a compound nucleus and will influence the pathway of non-compound reactions. Figure 1 depicts the topology of such a surface for a system of total mass and charge near those of ^{110}Sn.

Most fission studies do not explicitly consider the asymmetry coordinate but

0375-9474/87/$03.50

rather consider all near symmetric divisions as one decay channel. While there is some justification for this procedure for highly charged or rapidly rotating nuclei, where there is a deep symmetric valley in the potential, it is highly questionable when this feature in the potential is not present. Nevertheless, the asymmetry independent analyses have proven quite useful in that they provided the first evidence indicating the importance of a finite range (FR) correction to the standard rotating liquid drop (RLDM) barriers.[1-3] This correction amounts to a reduction of the symmetric RLDM barriers by approximately 25% in the A ~ 110 region.

More recently, the study of the emission of large fragments, intermediate in mass between alpha particles and symmetric fission fragments, from compound nuclear reactions, has been used to determine the emission barriers as a function of asymmetry.[4-6] This recent work utilized light ion systems and therefore the features of the potential energy surface examined are those in the low L-wave region. In the mass range of A ~ 110, the broad region where the barriers are independent of asymmetry (see Fig. 1) has indeed been verified by showing that the barriers for Z ~ 12 are very close to those deduced from a standard fission study[2], which considers fragments near symmetry. This agreement and an asymmetry dependent comparison of FR and RLDM barriers to

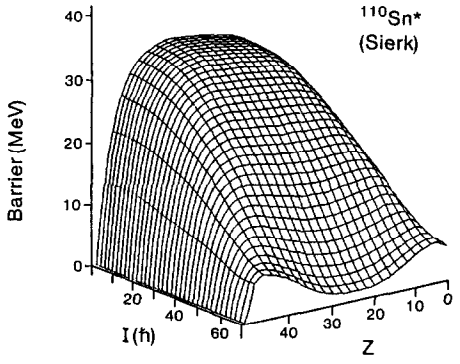

FIGURE 1
Surface plot of the asymmetry and angular momentum dependent barriers for the decay of ^{110}Sn* calculated with a finite range corrected rotating liquid drop model.

those deduced from the experimental data gave additional evidence of the importance of the FR correction.[6] Further asymmetry dependent studies have verified that the Businaro - Gallone transition does indeed occur in the vicinity of A ~ 100.[7]

The work discussed above, however, does not address the subject of the angular momentum dependence of the emission barriers. The present work does confront this issue by comparing the yields of large fragments, from both low and high angular momentum reactions, to equilibrium calculations which utilize angular momentum and asymmetry dependent emission barriers. These barriers are extensions of the previous work by Sierk[6] and are those shown in Fig. 1.

A second feature of the present work is a comparison of the experimental gamma ray multiplicity distributions ($M_\gamma(z)$) to transferred spin distributions calculated from the same equilibrium model used to predict the fragment yields. The barriers seen in Fig. 1 determine the L-wave fractionation (L-wave distribution contributing to each exit channel). These distributions, coupled with a rotation model, provide predictions of the transferred spin distribution for each asymmetry. The comparison of these distributions to the measured $M\gamma(z)$ distributions not only provides information on the rotation regime at the scission point but also on the width of the primary L-distributions corresponding to each decay channel.

II. EXPERIMENTAL METHODS

The new experimental data reported here involve the $^{45}Sc + ^{65}Cu$ system. Self-supporting ^{65}Cu target foils (enriched to 99.7% in the mass 65 isotope and 320-450 $\mu g/cm^2$ thick) were bombarded with a 200-MeV ^{45}Sc beam from the Holifield Heavy-Ion Research Facility. In this experiment the intermediate mass fragments were detected by two large solid angle telescopes with ion chambers as the ΔE detectors and Si(Li) as the E detectors. Each Si(Li) detector consisted of four strips (1.1 cm by 4.6 cm) that were position sensitive in the long direction. The telescopes subtended 18° in the laboratory system and each was centered at both 40° and 55° from the beam direction during the experiment.

The spin spectrometer served as the γ-ray detector and measured simultaneously the γ-ray multiplicity (M_γ), the total γ-ray de-excitation energy and the γ-ray angular correlations. In this experiment 70 of the 72 detectors were used, covering 94.5% of 4π sr. For each event triggered by either ion chamber the NaI pulse heights, NaI times as well as the ΔE, and E pulse heights, the silicon position, the e^- drift time in the ion chambers, and the time for each Si(Li) strip were recorded on magnetic tape. The data were processed to distinguish γ-rays from neutron pulses (utilizing time of flight information)

and to unfold the total γ-ray pulse height versus number of γ-ray hits (k) to yield total E_γ versus M_γ (see ref. 8 for the details of these procedures).

III. EXPERIMENTAL RESULTS

The angular distributions for the kinetic energy relaxed component for several representative elements are shown in Fig. 2. Due to the constraints imposed by the small scattering chamber inside the spin spectrometer and the large ion chambers, the angular distributions were obtained only over a modest angular region. Over this region, most of the angular distributions are compatible with a $1/\sin(\theta)$ function (solid lines). The distributions for the higher Z's do show some evidence for an enhanced forward peaking in excess of the $1/\sin(\theta)$ curves. This might suggest the presence of a non-rotationally relaxed component (deep inelastic scattering) which is important for the forward angular region for the heaviest, most symmetric elements. More extensive angular distributions for fission-like fragments have been reported for 200 and 215 MeV $^{35}Cl + {}^{62}Ni$. In that work[2], substantial agreement with a $1/\sin(\theta)$ distribution was observed for the symmetric mass fragments. In the present work we will compare only experimental differential cross-sections at $\theta_{CM} \sim 90°$ to equilibrium calculations. This is tantamount to assuming that there is not

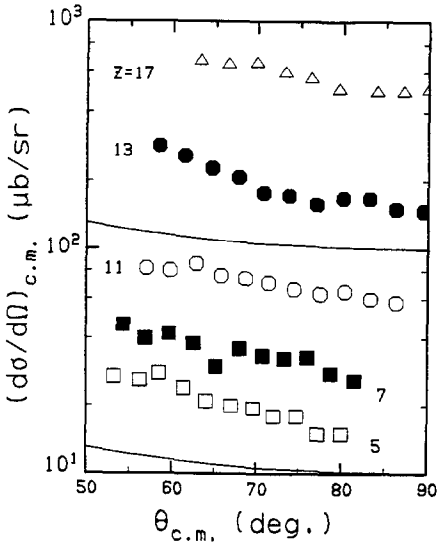

FIGURE 2
Center of mass angular distributions for B, N, Na, Al and Cl. Statistical errors are approximately indicated by the size of the symbols. The solid lines are $1/\sin(\theta)$ functions.

a significant contribution of other processes (DIC) contributing at $\theta_{CM} \approx 90°$, which is more than 25° behind the classical grazing angle.

The mean fragment energies ($E3_{CM}$) and total kinetic energies (TKE) for the energy relaxed component are shown in Figure 3 as a function of detected charge. The momentum balance was performed assuming that the mass associated with each charge was that derived by equilibrating the charge for a given mass split in a liquid drop model. These data have been corrected for sequential evaporation in the event-by-event analysis. This correction assumed that the available excitation energy was divided between the fragments in proportion to their masses, 12 MeV is removed per evaporated mass unit and that, on the average, the fragment velocity is unaltered by the evaporation process. These assumptions lead to the conclusion that the lightest fragments do not undergo any particle evaporation while the medium to heavy fragments evaporate 1 to 3 particles. The magnitude of the sequential charged particle evaporation can be examined for the symmetric region where we have coincidence data. The detectors were located symmetrically about the beam (either both at 40° or both at 55°) and therefore we only have coincidence data near symmetry. A contour plot of the probability of detecting fragments with atomic numbers Z_3 and Z_4 is shown in Fig. 4. This plot indicates that approximately 90% of the events near symmetry have no charged particle evaporation and what charge particle evapora-

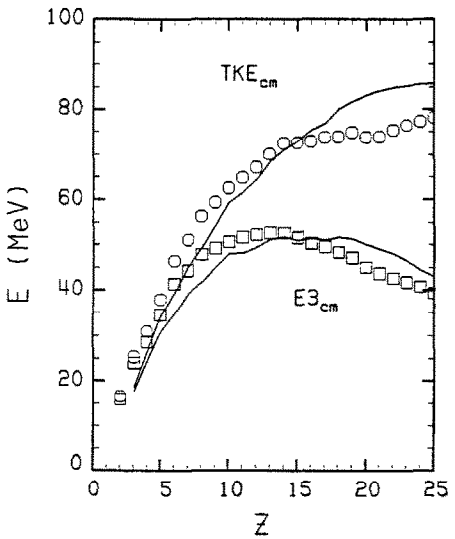

FIGURE 3
Center of mass mean energies as a function of atomic number. The solid line is the calculation described in the text.

tion there is, is protons. The overwhelming predominance of neutron evaporation from the secondary fragments agrees with standard evaporation calculations[9] at the estimated excitation energies of the primary fragments.

The differential cross sections, near $\theta_{CM} = 90°$, for fragments with atomic numbers between Z = 1 and Z = Z_{sym} are shown in Fig. 5 as the solid symbols. The cross section for Li is about a factor of 200 lower than that for α-particles. The cross sections remain at this relatively low value for elements lighter than Ne. For heavier elements, the cross sections steadily increase until a broad maximum is obtained near symmetry. We mention again that these data are the kinetic energy relaxed component and therefore these cross sections do not contain contributions from quasi-elastic or transfer reactions.

In the low cross section region (3 < Z < 11) a strong enhancement of fragments with even atomic numbers over fragments with odd atomic numbers is observed. Careful study of the cross sections indicates that the even enhancement continues up to Z = 20. Exhaustive evaporation calculations over the range of possible excitation energies of the primary fragments indicate that only small (<10%) enhancements of even atomic number fragments can result from

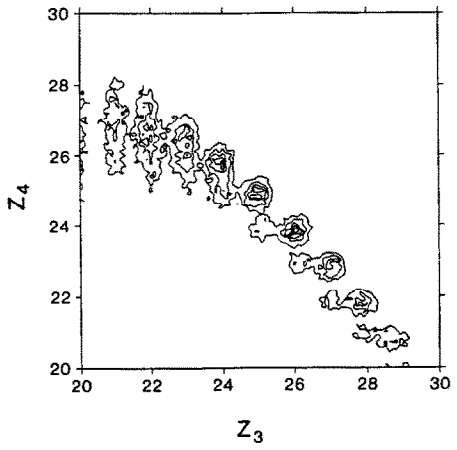

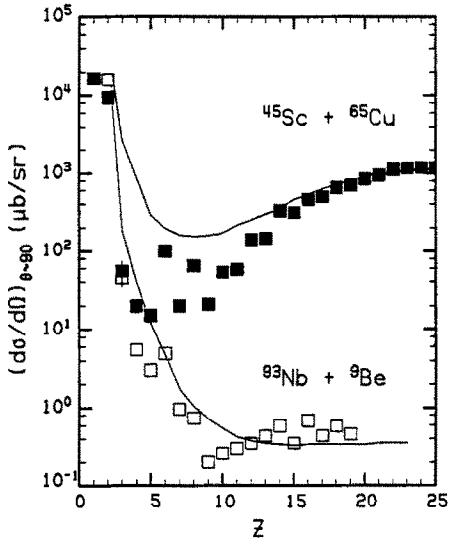

FIGURES 4 and 5

4. Contour plot of the probability of detecting two fragments, one with charge Z_3, the other with charge Z_4. The two detectors are at equal angles on opposite sides of the beam, therefore, the coincidence efficiency is large only over the near symmetric region.
5. Differential cross sections (angles indicated) for the $^{45}Sc + ^{65}Cu$ (solid symbols) and $^{93}Nb + ^{9}Be$ (open symbols) systems. The solid lines are the calculations described in the text.

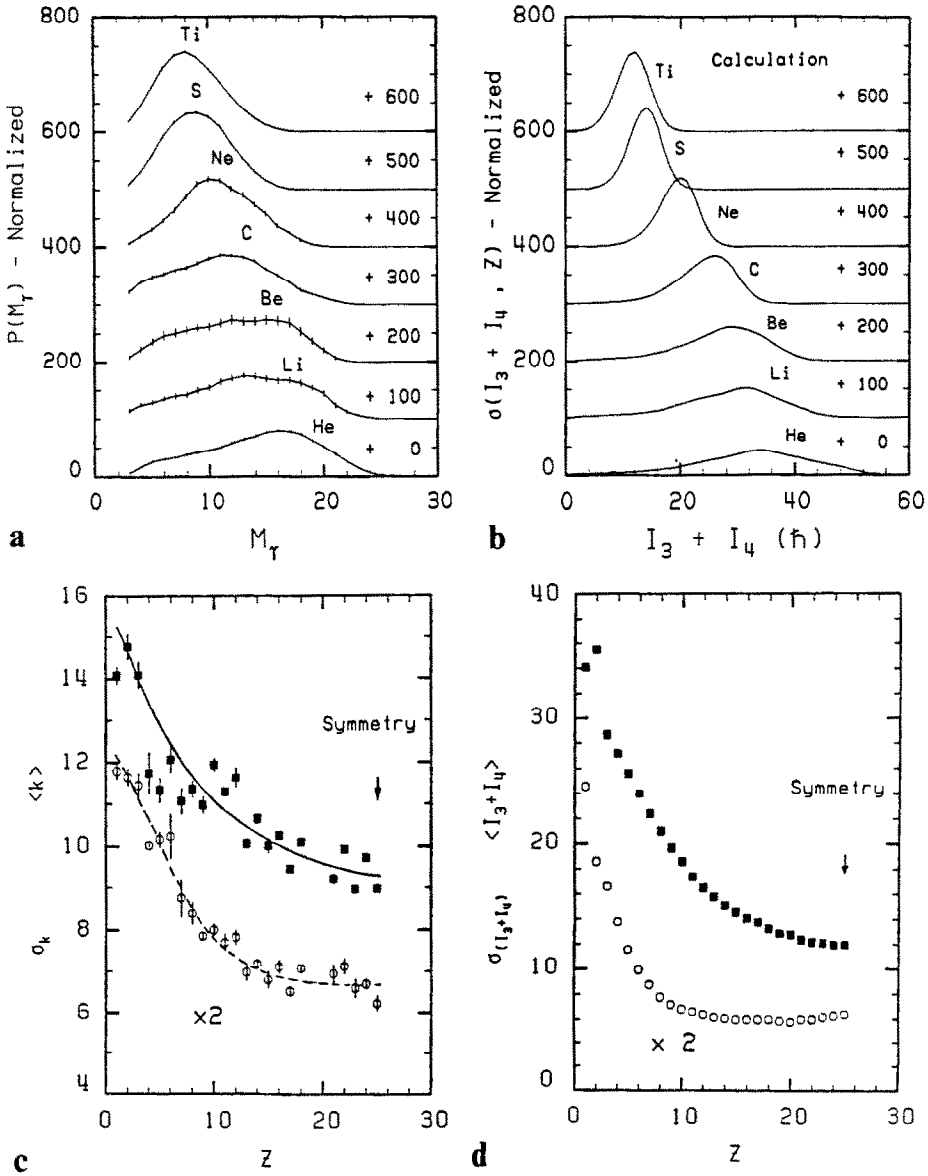

FIGURE 6

a) Experimental γ-ray multiplicity distributions (M_γ) in coincidence with He, Li, Be, C, Ne, S, and Ti fragments. The M_γ distributions have been normalized to 1000. The distributions have been shifted on the ordinate by the values indicated in the figure. b) Calculated transferred spin distributions for the same elements as (a). The curves are normalized and offset in the same fashion as for (a). c) First two moments of the experimental M_γ distributions shown in (a). d) First two moments of the calculated transferred spin distributions shown in b).

a sequential process. It should be realized that the total charge is even (50) and for that matter so is the total number of neutrons (60). Therefore, two body decay of a completely fused system results in even-even or odd-odd Z pairs. (It is interesting to note that very few of the low energy studies of fragment charge distributions have this feature. Most studies have used an even Z projectile and an odd, monoisotopic, Z target.) The occurrence of doubly even pairs suggests an explanation for the persistence of the even enhancement beyond the light Z region.

As mentioned earlier, the γ-ray data were analyzed to provide the total γ-ray energy, M_γ as well as the individual γ-ray energies. The M_γ distributions for selected elements are shown in Fig. 6a. The distributions for the lighter elements are broad with the most probable values being significantly greater than the average values. As the atomic number increases, the M_γ distributions become narrower and more symmetric and move to lower mean M_γ values.

In order to relate the γ-ray multiplicity distributions of Fig. 6a to transferred spin distributions we must investigate the distribution of γ-ray multipolarities emitted in the reaction. We have not undertaken a detailed study of this point, however we can answer the question of what asymmetry region is consistent with a preponderance of stretched E2 transitions.[10] Figure 7 shows the distribution of γ-rays in the plane perpendicular to the beam. The fragments were detected near $\theta_{CM} = 90°$ at an azimuthal angle of $\phi \approx 145°$. The γ-ray distributions for elements that are more than one charge removed from 8 show the distinctive stretched E2 form.[11] The distributions for nitrogen and fluorine indicate an increased proportion of multipolarities other than stretched E2 and that for oxygen shows no angular dependence at all. This variation of the multipolarity mixing is undoubtedly due to the influence of the N = 50 shell in the heavy partner. The complimentary fragment to ^{16}O is $^{92}Mo_{50}$ (the most probable sequential decay is 2n).

The similarity of the γ-ray angular distributions, when the fragment is not close in charge to oxygen, suggests that the functions that convert M_γ to transferred spin, $I_3 + I_4$, should be similar. On the other hand, around Z = 8, the conversion function may be substantially different.

IV. CALCULATIONS AND DISCUSSION

The purpose of the present work is to gain insight into the angular momentum dependence of large fragment production from compound nuclei. Unfortunately, the introduction of large L-waves inevitably raises the issue of the relative importance of faster reaction mechanisms where the mass asymmetry degree of freedom has not been completely explored. In order to minimize this problem we

have chosen a low beam energy and we will emphasize data far behind the classical grazing angle. For the 200 MeV Sc + Cu system, the Bass model[12] predicts that the critical L-wave for fusion is 70 ħ. Since the grazing L-wave is approximately 80 ħ, 75% - 80% of the reaction cross section is expected to fuse. Of the remainder, some fraction is quasi-elastic or transfer reactions and therefore is eliminated from our data by our relaxed energy requirement. The difficulty lies in a component that is kinetic energy relaxed but where the mass asymmetry degree of freedom is not. As stated above, we will emphasize the data at backward angles in order to bias against this deep inelastic component, which should be focussed around grazing angle. However, even with this bias, against what we suspect to be a small component, we cannot be confident that all of the detected large fragments result from compound nucleus decay. While the flat angular distributions do suggest a long-lived intermediate, angular distributions (even a $1/\sin(\theta)$ dependence) cannot be used to prove that the intermediate has lived long enough to equilibrate the mass asymmetry degree of freedom. Nevertheless, since the great bulk of the cross section must result from compound nucleus decay it is instructive to compare these data to equilibrium calculations.

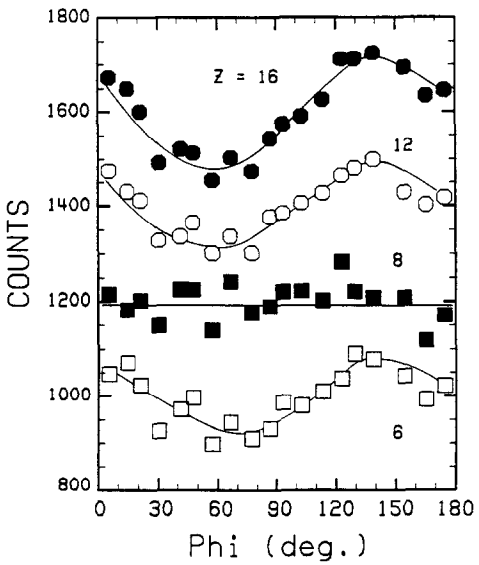

FIGURE 7
Angular distribution of γ-rays emitted in the plane perpendicular to the beam for events triggered by fragments detected at $\phi = 145°$. Statistical errors are indicated by the size of the data points. Systematic errors, in the efficiencies of individual NaI's, which are larger than the data points are present. The lines are drawn to guide the eye.

A. Statistical Model

The model used here is similar to that used in previous complex fragment emission studies.[4,5,7] This model is an extension of the traditional fission, transition state formalism to explicitly treat the mass asymmetry coordinate. This model was originally suggested by Moretto[13] and more recently by Swiatecki.[14] This model, with a few minor changes, has also been used recently in an effort to understand large fragment production in intermediate energy systems (35 MeV/nucleon ^{86}Kr + ^{12}C, ^{17}Al; ref. 15).

The initial angular momentum distribution of the compound system is taken as a diffuse triangle,

$$\sigma_{CN}(L) = \pi\lambda\!\!\!^{-2}\, F(L)\, (2L+1), \tag{1}$$

where F(L) is a Fermi function,

$$F(L) = \frac{1}{1 + e^{(L-L_h)/L_d}}\ .$$

The value of L_h is the minimum of the critical angular momentum for fusion[12] and the maximum possible angular momentum in the system, taken as that for a grazing collision. The diffuseness is taken as $2\hbar$. The cross section for each charge is calculated from

$$\sigma_Z(L) = \sigma_{CN}(L)\ \Gamma_Z(L)\ /\ \Gamma_{TOT}(L) \tag{2}$$

where

$$\frac{\Gamma_Z}{\Gamma_n} = \frac{T_Z}{T_n}\left[\frac{E^*_{CN}(L) - B_n}{E^*_{CN}(L) - B_Z(L)}\right]^2 \exp\{2[a(E^*_{CN}(L) - B_Z(L))]^{1/2} - 2[a(E^*_{CN}(L) - B_n)]^{1/2}\}$$

The excitation energy of the compound system is given by $E^*_{CN}(L) = E_{cm} + Q - E^{rot}(L)$, where $E^{rot}(L)$ is the rotating ground state energy as determined by the rotating liquid drop model. The temperatures are calculated from the available excitation energy, $U = E^* - B = aT^2$ with $a = A_{TOT}/7.1$ MeV^{-1} (ref. 16). The angular momentum and mass asymmetry dependent barriers, $B_Z(L)$, come from the FR calculation while the neutron binding energy (B_n) is from a LDM.

The main difference between these calculations and those reported in previous works[4,5,7] is that the mass asymmetry and angular momentum dependent barriers for fragments with Z > 2 come from a finite range corrected liquid drop model rather than from a sphere-sphere or a spheroid-spheroid model. This improvement removes the distance between centers of the nascent fragments as a free parameter. This variable was adjusted in previous works in order to obtain agreement between the experimental TKE and the sum of the Coulomb and relative rotational energies of the fragments. Since we do not have this para-

meter in the present work, we can then compare not only the fragment cross sections but also the kinetic energies to the model calculations.

A minor modification in the model calculation is that the multi-step emission is now considered. Emission from any of the light particle decay products in a 5(Z) x 5(N) block of the Segre chart (CN in upper right hand corner) is considered. With the exception of the light particle cross sections and the highest energies of the excitation functions, this amounts to less than a 15% correction.

TABLE 1

System	E_{lab} (MeV)	CN	E^* (MeV)	(1) L_c ($\hbar$)	(2) L_m	(3) x	(4) y (L)	ref.
$^{3}He + ^{nat}Ag$	45	^{111}In	60	13	20	0.43	0.01 (13)	4,5
	60		74	15	24		0.01 (15)	
	70		84	17	26		0.01 (17)	
	90		103	19	31		0.01 (19)	
	130		142	24	38		0.02 (24)	
$^{93}Nb + ^{9}Be$	782	^{102}Rh	78	34	43	0.40	0.05 (34)	7
$^{35}Cl + ^{62}Ni$	155	^{97}Rh	86	59	68	0.42	0.16(59)	2
	160		89	62	71		0.18(62)	
	165		92	64	74		0.19(64)	
	170		95	65	77		0.20(65)	
	200		115	73	91		0.25(73)	
	215		124	78	97		0.28(78)	
$^{45}Sc + ^{65}Cu$	200	$^{110}_{50}Sn$	94	70	80	0.45	0.12(60)	present
							.17(70)	work
							.22(80)	

(1) The critical angular momentum for fusion given by the Bass model.[12]
(2) The maximum angular momentum for a grazing collision.
(3) $x = Z^2/50A$
(4) $y = 2L^2/A^{7/3}$

B. Particle Yields and Energies

Table 1 lists several systems in the mass 100 region which can be used to test our model calculations. The systems include 2 low angular momentum systems, $^{3}He + ^{nat}Ag$ and $^{93}Nb + ^{9}Be$ and two high angular momentum systems, $^{35}Cl + ^{62}Cu$(2) and $^{45}Sc + ^{65}Cu$. The low angular momentum systems are sensitive to the portion of the barrier surface which is insensitive to asymmetry over the central region, while the high angular momentum are sensitive to the whole

surface shown in Fig. 1.

Cross sections for individual elements are not reported for the $^{35}Cl + ^{62}Ni$ system so we will not make a detailed comparison for these data. However, this work[2] does report both the evaporation residue cross section (σ_{ER}) and the yield of symmetric fragments, which we will call σ_f, as was done in ref. 2. The measurement of both cross sections allows us to check the angular momentum window used in the calculation (Bass model) against the experimentally determined L_{cr}, as well as the symmetric fission cross section. This comparison is made in Table 2. The values of L_c(Bass) are within 2 $\hbar$ of those determined from the data. In fact, the predicted σ_{CF} are within the experimental uncertainties. This provides some confidence that the angular momentum windows used in the present work are appropriate. The values of σ_f are calculated by summing the yield from Z = 10 to Z_{sym}. (The lower limit in the sum is not that important since the cross sections are decreasing steeply with decreasing Z.) The calculated cross sections agree with the experimental values and the reported uncertainties for 5 out of the 6 determinations. The sixth cross section deviates by 2 times the quoted error.

TABLE 2

Cross sections and critical angular momenta for the $^{35}Cl + ^{62}Ni$ system.

	E_{lab}(MeV)					
	155	160	165	170	200	215
			Data[2]			
σ_{ER}		998 ± 70	1089 ± 76	1091 ± 76	960 ± 70	956 ± 70
σ_f (data)	45 ± 9	78 ± 15	114 ± 22	126 ± 24	340 ± 100	420 ± 85
L_c ($\hbar$)	59	60	64	66	74	79
			Calculation			
L_c (Bass)	59	62	64	65	74	78
σ_f (calc)	27	72	117	142	367	452

The calculated differential cross sections, at $\theta_{cm} = 90°$, for both the $^{93}Nb + ^{9}Be$ and the $^{45}Sc + ^{65}Cu$ systems are shown in Fig. 5 as solid lines. For comparison the differential cross sections, for large θ_{CM}, are also shown for both systems. As is the case for the $^{35}Cl + ^{62}Ni$ excitation function, the calculation reproduces the yield of large, near symmetric, fragments. On the other hand, the calculation overpredicts the yields of light fragments, $3 < Z <$

11. For the $^{93}Nb + ^{9}Be$ system, the overprediction is slight and one might consider it insignificant in light of the assumptions in the calculation. However, for the $^{45}Sc + ^{65}Cu$ system the overprediction is quite large, as much as a factor of 5 in the Z~7 region.

While the successes of the model calculations are considerable, we are drawn to examine the possible reasons for the failure in the light Z region. The likely explanations are an underprediction of the high angular momentum barriers for atomic numbers Z~7 or that the application of an equilibrium calculation to the high angular momentum case is inappropriate. If the barriers are underpredicted for large angular momenta this should be reflected in the fragment energies.

The mean kinetic energies can be calculated from the difference between the barrier energy and that for the separated fragments.

$$\langle TKE_Z \rangle = Q_Z^{out} + \langle E_{CN}^{rot} \rangle + \langle B_Z \rangle + 2\langle T_Z \rangle - \langle E_3^{rot} \rangle - \langle E_4^{rot} \rangle - \langle E_{diss} \rangle. \qquad (3)$$

The brackets indicate averages over angular momentum, Q^{out} is the exit channel Q_{value} and the intrinsic rotational energies of the compound nucleus and the two exit channel fragments are given by E_{CN}^{rot}, E_3^{rot}, and E_4^{rot}, respectively. Equation 3 uses 2T as an estimate of the mean kinetic energy in the decay mode, as well as contributing the relative rotational energy to the kinetic energy. Some of the available energy should be dissipated back in fragment excitation.[17] This is represented by E_{diss}.

In order to evaluate the rotational energy correction terms in equation 3 (E_3^{rot} and E_4^{rot}) we must assume a rotation model in order to divide the angular momentum into the intrinsic and relative components. We assume that the intermediate rotates rigidly. The rotating ground state energies themselves are calculated from the RLDM. The dissipated energy is not included in the calculation. The value of this term is quite uncertain in that it depends on the hydrodynamics of the scission process. It can, however, be estimated for symmetric division from the work of Nix (Fig. 13 of ref. 17). The predicted value of $\langle E_{diss} \rangle$ is roughly 8 MeV for a fissility parameter of x = 0.45 and it increases to near 18 MeV for x = 0.60. While the systems discussed here have x ~ 0.45 the value of x = 0.60 may be more appropriate for the high angular momentum systems.

The calculated values of TKE and E_3 are shown as solid lines in Fig. 3. The calculated energies are low for large asymmetries (light elements) and about 9 MeV greater (in TKE) than the data near symmetry. As just mentioned, the calculation should exceed the actual energies by the dissipated energy. While

this is true near symmetry, the calculation fails for large asymmetries. As is the case for the fragment yields, this discrepency suggests that the barriers are underpredicted for the large angular momentum asymmetric channels. Further support for this conclusion can be obtained from a comparison of the calculated barriers in the asymmetric mass region to those determined from the ^{3}He + Ag excitation function.[5,6] Furthermore, since it is unreasonable to suspect that the barriers could be low by more than about 5 MeV, Fig. 3 indicates that $\langle E_{diss} \rangle$ must decrease with increasing asymmetry.

C. Transferred Angular Momentum Distributions

Investigation of the angular momentum transferred to intrinsic spin in heavy ion reactions has been an active research area for a decade. The most common tool for these investigations has been the measurement of the mean gamma-ray multiplicity for a given exit channel. With some uncertainty, mostly associated with the multipolarity mixing, the $\langle M_\gamma \rangle_Z$ can be converted to $\langle I_3 + I_4 \rangle_Z$. In some cases a second moment is also extracted from M_γ measurements. In the present work, we go a step further and present the complete experimental M_γ distributions for each Z (rather than just the first one or two moments) and compare them to calculated $I_3 + I_4$ distributions. The experimental $M_\gamma(Z)$ distributions are shown in Fig. 6a and were discussed in the previous section.

The calculated L-wave fractionation is shown in Fig. 8. As the decay channel asymmetry decreases, the contributing L-wave distribution moves to larger

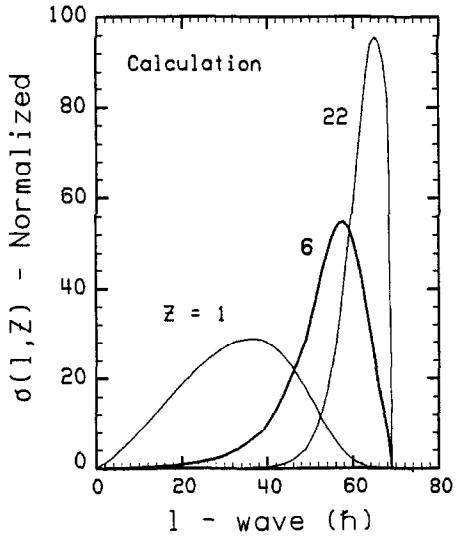

FIGURE 8
Calculation of the initial l-wave distributions for selected exit channels.

average values and becomes narrower. These trends can be understood by inspecting Fig. 1.

The division of these total angular momentum distributions into intrinsic and relative components requires a rotation model. As we did for the fragment energy, we assume rigid rotation of the intermediate. For this purpose we modelled the intermediate as two separated spheres. We have also included fluctuations in the transferred spin.[18] The resulting calculated $I_3 + I_4$ distributions are shown in Fig. 6b. The rigid rotation model inverts the distributions from those in Fig. 8. (High Z value with large mean L values have low mean $I_3 + I_4$ values while low Z values with low mean L values have high mean $I_3 + I_4$.) This is the feature which has been used previously to suggest that rigid rotation is achieved in deep inelastic reaction.[19-21] On the other hand, the trend in the widths is preserved. (Low Z values have broad distributions while high Z values have narrow distributions.)

Comparisons of the experimental distributions and their moments, Fig. 6a and 6c, to the calculated ones, Fig. 6b and 6d, indicates that the model does reproduce the main experimental features. The agreement between the trends in first moments of these distributions supports the rigid rotation model. (This is neither new nor surprising.) The favorable comparison between the calculated and experimental second moments does indicate that the larger the fragment (more symmetric the decay) the narrower is the contributing primary L-wave distribution. (This is new, but not surprising if one believes in the equilibrium formalism used here.) Furthermore, the conversion from M_γ to $I_3 + I_4$ is slightly less than a multiplicative factor of 2. This is to be expected when the majority of γ-rays are quadrupole transitions. As shown in the previous section, the angular distributions support this contention, except when one of the fragments has $N \sim 50$.

D. The Even-Odd Effect

Before concluding we would like to comment on an interesting even-odd Z effect that we observed. We found that the relative yields of odd atomic number elements could be enhanced by selecting low gamma-ray fold (k) and, conversely, that the yields of even Z elements could be enhanced by selecting high gamma-ray folds. This is shown in Fig. 9. This effect is readily understood when the k distributions for neighboring elements are compared, Fig. 10. The k distributions for the odd Z elements are shifted down by a few units. This shift can be explained if the initial L-wave populations, Fig. 8, and the transferred spin distributions, Fig. 6, are blind to the ground state structures of the fragments. Neighboring elements will have nearly identical L-wave

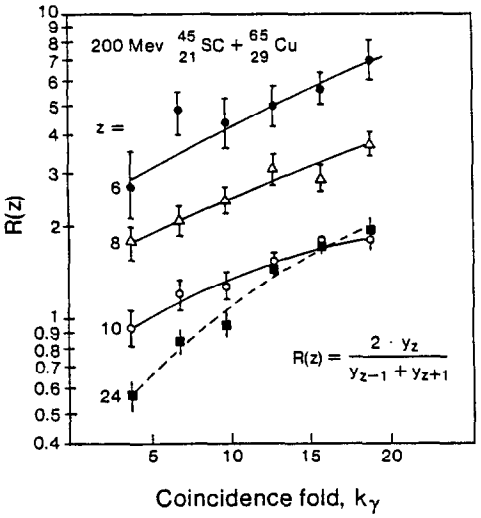

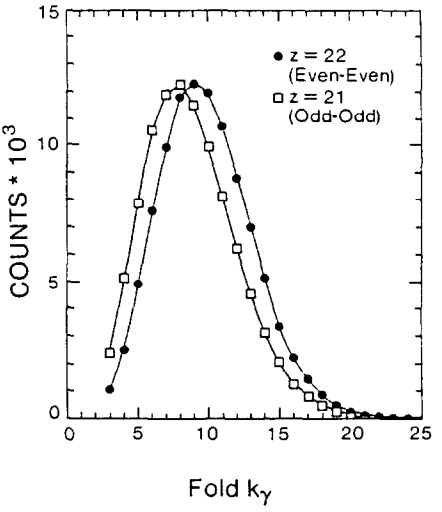

FIGURES 9 AND 10

9. The relative yield of even Z elements to the sum of the neighboring odd Z elements as a function of γ-ray fold, k.
10. The γ-ray fold distributions for an even Z element and a neighboring odd Z element.

distributions and nearly identical transferred spin distributions. However, the odd-odd channels will have fewer γ-rays due to the ground state spins. In essence, this effect is due to the fact that the bulk of the angular momentum is transferred to orbital and not to intrinsic fragment spin. As a result the sum of the ground state spins are not insignificant compared to the total transferred spin.

CONCLUSIONS

We have used low energy reactions in an effort to study the features of the fragment-fragment potential energy surface. This study has verified the main features of the PES calculated by a liquid drop model for $A_T \sim 110$. Specifically, at low spin the surface or emission barriers are rather independent of mass asymmetry while for large spins a strong preference for symmetric decay develops. There was no reason to resort to a reaction mechanism that is not equilibrated in the mass asymmetry degree of freedom (such as DIC).

Detailed comparison of the yields from three systems (Sn + Cu, Nb + Be, and the excitation functions of ^{3}He + Ag) as well as fragment energies indicates

that the finite range rotating liquid drop model slightly under-predicts the asymmetric barriers in the vicinity of $Z \sim 7$. In addition, some rather limited evidence has been presented that argues for a decrease in the saddle to scission energy dissipation with increasing asymmetry in the decay mode.

Finally, the coincident gamma-ray multiplicity distributions not only confirm that the angular momentum is partitioned as expected by a rigidly rotating critical decay shape but also that the greater the symmetry in the decay channel the narrower is the contributing primary L-wave distribution.

This work was supported in part by the U.S. Department of Energy under contracts DE-AC02-86ER40210, DE-AS02-76ER04052, and DE-AC05-84OR21400. One of us (L.G.S.) is pleased to acknowledge support from a U.S. Presidential Young Investigator Award. Oak Ridge National Laboratory is operated by Martin Marietta Energy Systems Inc.

REFERENCES

1) G. Anderson et al. Z. Phys. A293 (1979) 241.
2) M. Blann and T.T. Komoto, Phys. Rev. C26 (1982) 472; B. Sikora et al. Phys. Rev. C25 (1982) 1446.
3) F. Plasil et al. Phys. Rev. C29 (1984) 1145.
4) L.G. Sobotka et al. Phys. Rev. Lett. 51 (1983) 2187.
5) M.A. McMahan et al. Phys. Rev. Lett. 54 (1985) 1995.
6) A.J. Sierk, Phys. Rev. Lett. 55 (1985) 582.
7) L.G. Sobotka et al. Phys. Rev. Lett. 53 (1984) 2004.
8) M. Jääskeläinen et al. Nucl. Instr. and Meth. 204, (1983) 385.
9) A. Gavron, Phys. Rev. C21 (1980) 230.
10) We use the word consistent because we cannot distinguish between stretched E2 and non-stretched ($\Delta I = 0$) dipole transitions.
11) Z. Majka et al. Phys. Rev. Lett. 58 (1987) 322.
12) R. Bass, Phys. Rev. Lett. 39, (1977) 265.
13) L.G. Moretto, Nucl. Phys. A247 (1975) 211.
14) W.J. Swiatecki, Austr. J. Phys. 36 (1983) 641.
15) F. Auger et al. Phy. Rev. C35 (1987) 190.
16) J.R. Huizenga and L.G. Moretto, Ann. Rev. Nuc. Sci. 22 (1972) 427.
17) J.R. Nix, Nucl. Phys. A130 (1969) 241.
18) R.P. Schmitt and A.J. Pacheco, Nuc. Phys. A379 (1982) 313.
19) P. Glässel et al. Phys. Rev. Lett. 38, (1977) 331.
20) M.N. Namboodiri et al. Phys. Rev. C20 (1979) 982.
21) L.G. Sobotka et al. Nucl. Phys. A371 (1981) 510.